Transition dynamics in the electrical breakdown of the quantum Hall effect

Ming-Yang Li,[1] T. Nakajima,[2] Kuan-Ting Lin,[1] C. C. Chi,[1] J. C. Chen,[1] and S. Komiyama[2]
[1]*Department of Physics, National Tsing-Hua University, Hsinchu, Taiwan 30013, Republic of China*
[2]*Department of Basic Science, University of Tokyo, Komaba, Tokyo 153-8902, Japan*
(Received 7 December 2011; revised manuscript received 5 April 2012; published 21 June 2012)

We investigate the dynamic properties of the breakdown of integer quantum Hall states (QHSs). The critical field of QHS breakdown that occurs at a filling factor of $\nu \sim 2$ is found to depend on the scan rate of the applied Hall field E_H and to fluctuate stochastically; in contrast, a smooth breakdown is observed at $\nu \sim 4$. The histogram of the critical values of E_H can be used to derive the escape and relaxation time, ranging from a few seconds to 10 μs between the low-dissipation QHS and the dissipation state. The increase of the escape rate between the low-dissipative QHS and the dissipative state is accompanied by a decrease of the relaxation rate and vice versa, indicating the bistable nature of the breakdown phenomena. The observed results agree well with the calculated results based on the basis of the bootstrap electron heating model. We conclude that the dynamic behaviors of QHS breakdown are governed by the transition probability that resides in the thermal bistable regime between the QHS and the dissipation states.

DOI: 10.1103/PhysRevB.85.245315 PACS number(s): 73.43.−f

I. INTRODUCTION

The integer quantum Hall effect (IQHE) is characterized by the quantization of Hall conductivity σ_{xy} to integer multiples of e^2/h, accompanied by a vanishing diagonal conductivity σ_{xx}.[1,2] When the Hall electric field E_H (or the sample current density) increases beyond a critical value, σ_{xx} abruptly increases and the dissipation-less QHS breaks down.[3,4] The breakdown phenomenon not only reflects the nature of IQHE, but also hinders the application of the effect as a highly precise resistance standard; consequently, the collapse of the QHE attracts substantial research attention.[3–22] Experimental evidence indicates that the breakdown of the QHE is accompanied by a sudden increase in the local electronic temperature T_e. Accordingly, many proposed theoretical models have been devoted to the elaboration of the roles of T_e and E_H in the breakdown. Significant theoretical effort has focused on the effects of $E_H(r)$ on the local conductivity $\sigma_{xx}(r)$.[5,13,21] Nevertheless, recent experiments have revealed a length dependence of the breakdown process, providing convincing evidence that $\sigma_{xx}(r)$ is not influenced directly by $E_H(r)$.[23–25] To date, it is widely accepted that σ_{xx} is mainly governed by T_e, that is, $\sigma_{xx}(r) = \sigma_{xx}(T_e(r))$, and the breakdown is associated with the thermal bistability of T_e.[26]

The bistability of T_e can be understood in terms of the electron heating model. The dependence of T_e on E_H can be derived from the balance condition between energy gain rate and loss rate with the increase of E_H, as illustrated in Fig. 1.[27] The T_e-E_H plot displays a S-shaped diagram bounded by a lower critical field E_{LC} and an upper critical field E_{UC}. As $E_H < E_{\mathrm{LC}}$ or $E_H > E_{\mathrm{UC}}$, the electron system remains in a stable QHS at $T_e = T_{\mathrm{LS}}$ or in a stable dissipation state at $T_e = T_{\mathrm{HS}}$, respectively. Within $E_{\mathrm{LC}} < E_H < E_{\mathrm{UC}}$, where $\partial T_e/\partial E_H < 0$ holds, the intermediate T_e state ($T_e = T_{\mathrm{US}}$) is unstable against infinitesimal fluctuations; hence, a transition between the stable T_{LS} state and the T_{HS} state can be easily induced. It should be noted that $T_e(E_H)$ is a multifunction within the bistable regime; consequently, $T_e(r)$ at a given r depends not only on the value of E_H, but also on how E_H is applied. Experimentally, the width of the bistability regime $E_{\mathrm{UC}} - E_{\mathrm{LC}}$ is a material parameter that varies for different wafers.

The exact link between the thermal bistability and the observed breakdown phenomenon remains controversial. As an example, the threshold of the breakdown field E_{th} observed in the experiments is often found to be substantially lower than the theoretically expected upper critical field E_{UC}. Buss *et al.* argued that this phenomenon can be explained by a pre-breakdown mechanism, attributing it to a frequency-dependent hopping conductivity.[7] Alternatively, Nakajima *et al.* suggested that the transition probability from the T_{LS} state to the T_{HS} state is sufficiently high, even if E_H is much lower than E_{UC}; hence, the lower E_{th} is observed in a finite measurement time.[28] Moreover, various distinct breakdown behaviors have been observed in a number of experiments, including a hysteresis effect as the current or magnetic field is ramped,[3,4,6,7,22] telegraph-like fluctuations between the dissipationless states and the breakdown states,[4,8,9] and smooth single- or multistep transitions.[3,10] It is unclear how these apparently conflicting views and observations can be reconciled with thermal bistability. An understanding of the transition dynamics would provide a key to the clarification of the origin of the QHS breakdown.

In this paper we specifically investigate the dynamic properties of the QHS breakdown. We argue that within the entire bistable regime ($E_{\mathrm{LC}} < E_H < E_{\mathrm{UC}}$) the electron system can occupy either the T_{LS} state or T_{HS} state. The probability of finding each stable state can be characterized by its corresponding lifetime: τ_L for the T_{LS} state and τ_H for the T_{HS} state. In general, the lifetime τ_L/τ_H as a function of E_H can be expected to start at $\tau_L = \infty$ ($\tau_H = 0$) at $E_H = E_{\mathrm{LC}}$ and rapidly decrease (increase) to $\tau_L = 0$ ($\tau_L = \infty$) at $E_H = E_{\mathrm{UC}}$. A well-known feature of this bistability is the stochastic nature of the T_{LS} state $\rightleftharpoons$ T_{HS} state transition process.[27,29,30] Here we present comprehensive measurements to explicitly extract τ_L and τ_H for values of E_H in the bistable regime. We reveal that the way in which the transition is triggered and its measurement would give rise to various features of resistance fluctuation during QHS breakdown. Our results bridge the

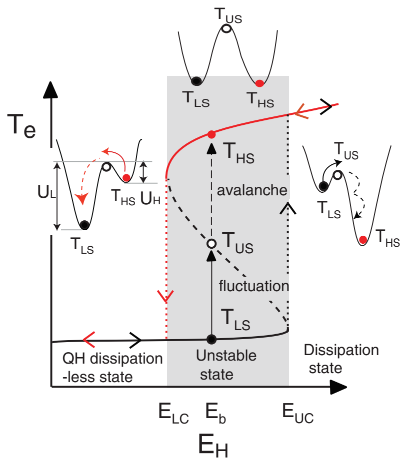

FIG. 1. (Color online) The curve of T_e vs E_H, obtained by the balance between the energy-gain rate and the energy-loss rate.[17] The insets show schematic diagrams of the E_H dependence of a bistable potential, adopted to model the breakdown process.

present understanding of the bistability of $T_e(E_H)$ to numerous experimental observations. Finally, we employ a theoretical simulation based on the electron-heating model to substantiate our findings.

II. EXPERIMENTS

The samples are fabricated from a GaAs/Al$_x$Ga$_{1-x}$As heterostructure crystal with a two-dimensional electron system. To characterize the samples we measure the Shubnikov–de Hass (SdH) oscillations with the applied magnetic field B to determine the carrier density n_s and the mobility μ at a temperature of 4.2 K. Two types of sample geometries, the Hall-bar geometry and the Corbino geometry, are investigated. The main features of the samples are listed in Table I. In this paper the presented results are primarily obtained from S2. The data obtained from S1 have been published elsewhere.[28] The lattice temperature is estimated to be $T_L \sim 300$ mK. The circuit scheme of the experimental setup is shown in the inset of Fig. 2(a). The Corbino sample is biased through a voltage source V_{SD} and the source-drain current I_{SD} is measured through a current-preamplifer. The longitudinal conductance can be derived from $\sigma_{xx} = I_{\mathrm{SD}}/V_{\mathrm{SD}} \times \ln(r_{\mathrm{out}}/r_{\mathrm{in}})/2\pi$, where r_{out} and r_{in} represent the outer and inner radii of the Corbino disk, respectively.

TABLE I. Specifications of the samples used in the experiments. Sample S1 is of Hall-bar geometry. S2 and S3 are of Corbino geometry. W is the width of the device, L is the separation between voltage probes of Hall-bar device, r_{in} is the inner radius of the Corbino device, n_s is the electron density, and μ is the electron mobility at 4.2 K.

Sample		S1	S2	S3
W	μm	100	60	30
L or r_{in}	μm	200	150	150
n_s	$\times 10^{15}$ m^{-2}	2.79	2.96	2.91
μ	m^2/V s	44	29.3	31.1

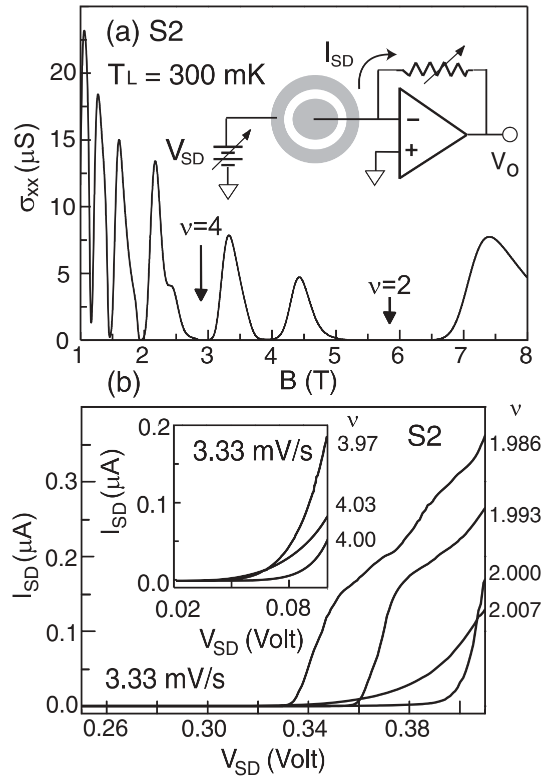

FIG. 2. (a) Shubnikov–de Hass oscillations of sample S2 measured at $T_L = 0.3$ K. The inset shows the schematic diagram of the measurement circuit. (b) The current-voltage (I_{SD}-V_{SD}) characteristics around the filling factor $\nu \sim 2$. The insert shows the I_{SD}-V_{SD} curves around $\nu \sim 4$.

Figure 2(a) show an exemplary trace of the Shubnikov–de Haas (SdH) oscillations of S2 with $V_{\mathrm{SD}} = 50\ \mu$V. The current-voltage curves of Fig. 2(b) display the electrical breakdown of the QHS in the vicinity of the filling factors $\nu = 2$ ($B = 5.82$ T) and $\nu = 4$ ($B = 2.91$ T). As V_{SD} ramps up slowly at $\sim$3.33 mV/s, I_{SD} sharply increases at a critical value of V_{SD}. The I_{SD}-V_{SD} curves in Fig. 2(b) show the $\nu \sim 2$ case, and the figure inset shows the $\nu \sim 4$ case, which exhibits a continuous single value.

To explore the dynamic behaviors of the breakdown, two different V_{SD} scanning schemes are adopted: the up-scan scheme and the down-scan scheme, as illustrated by the black solid line and red dashed line of Fig. 3(a), respectively. The scan rate is defined to be $dV_{\mathrm{SD}}/dt = W dE_H/dt = V_{\max}/\tau_{\mathrm{scan}}$, where $V_{\max}$ is set to ensure that the dissipation state can be studied. To prevent the crosstalk and noise from outside sources, one of the twisted pair wires are grounded. The twist-pair wires plus the external coaxial cable contributes $\sim$56 pF. The input capacitance of the homemade current preamplifier is about 20 pF. The capacitances of the Corbino device is less than 0.1 pF. The τ_{scan} parameter is limited by the total parasitic capacitance of the system ($\sim$78 pF) and the bandwidth of the preamplifier ($\sim$100k Hz). The minimum value of τ_{scan} is approximately 10 μs, which is restricted by our measurement circuit.

Figures 3(b)–3(d) summarize the I_{SD}-V_{SD} traces obtained by different scan schemes and scan rates, where the traces

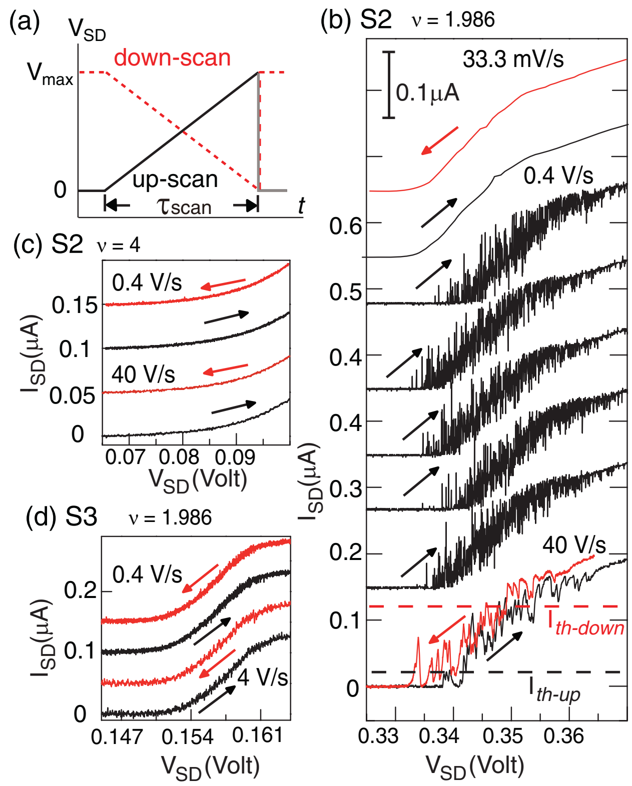

FIG. 3. (Color online) (a) Schematic diagrams representing the driving waveform of V_{SD}. The black and red lines represent the up-scan and down-scan schemes, respectively. (b) I_{SD}-V_{SD} characteristics of S2 at approximately $\nu \sim 2$ and (c) at ~ 4 for different scan rates. The black arrow indicates the up-scan and the red arrow indicates the down-scan. The black and red dashed lines indicate the defined current threshold for the up-scan and down-scan. (d) I_{SD}-V_{SD} traces of S3. Each trace is offset for clarity.

shown in Figs. 3(b) and 3(c) are from S2, and the trace in Fig. 3(d) is from S3. Each individual curve records a single scan of V_{SD}. As the scan rate of V_{SD} increases, the different behaviors of I_{SD} become visible for S2 at $\nu \sim 2$, as displayed in Fig. 3(b). At a scan rate of 0.4 V/s, the I_{SD}-V_{SD} characteristic fluctuates from one scan to another. Noisy spikes of I_{SD} that resemble random telegraph-like switching behavior are observed for the values of V_{SD} that fall within the breakdown regime. Moreover, the onset of the breakdown voltage varies in each run. At $\nu \sim 2$, the fluctuation width is $V_{\mathrm{SD}} \sim 16$ mV at 40 V/s and $\sim$12 mV at 0.4 V/s. Note that the threshold V_{SD} of the breakdown for the down-scan at 40 V/s is lower than that of the up-scan. We found that the appearance of the unstable features in I_{SD} is only dependent on the scan rate. The observed stochastic nature of the fluctuations provides direct evidence for the bistability of the breakdown event. In contrast, the fluctuation of I_{SD} is invisible for S2 at $\nu \sim 4$ and for S3 with smaller a channel width. Neither hysteresis nor switching behaviors are observed in the I_{SD}-V_{SD} curves, shown in Figs. 3(c) and 3(d).

To quantitatively evaluate the fluctuating characteristics, we wish to experimentally extract the time scales associated with the transient processes. As E_H increases steadily to a critical value E_{th}, the T_{LS} state with $\sigma_{xx} = 0$ has a chance to switch to the T_{HS} state with finite $\sigma_{xx} \neq 0$. Because the fluctuation-induced breakdown occurs as a random event with an average rate that depends on E_H, the value of E_{th} assumes random values with a certain switching probability distribution $P(E_H)$. The $P(E_H)$ distribution is defined by the condition that the probability that E_{th} will occur between E_H and $E_H + dE_H$ is $P(E_H)dE_H$. Therefore, the probability for the T_{LS} state $\rightarrow$ T_{HS} state transition over dt for a given dE_H can be expressed as $P(E_H)dE_H = (dt/\tau_L)[1 - \int_0^{E_H} P(u)du]$. Hence, the escape rate $1/\tau_L$ can be derived from the probability of escape in the interval from E_H to $E_H + dE_H$ for scanned at a certain rate dE_H/dt:[30]

$$\frac{1}{\tau_L(E_H)} = \left(\frac{dE_H}{dt}\right) \frac{P(E_H)}{1 - \int_0^{E_H} P(u)du}. \tag{1a}$$

Likewise, one can derive $1/\tau_H$ as

$$\frac{1}{\tau_H(E_H)} = \left(\frac{dE_H}{dt}\right) \frac{P(E_H)}{\int_0^{E_H} P(u)du}. \tag{1b}$$

The $P(E_H)$ distribution is normalized to unity such that $\int_0^{E_H} P(u)du$ expresses the probability of finding the T_{HS} state. The scan rate dE_H/dt is a control parameter in the experiment, and $P(E_H)$ can be obtained by constructing a histogram diagram by counting the variations of E_{th} with sweeping V_{SD}. The escape rates$1/\tau_L$ and $1/\tau_H$ can then be derived experimentally.

To determine τ_L and τ_H, E_{th} is recorded in each I_{SD}-V_{SD} trace in Fig. 3(b), based on the defined current threshold $I_{\text{th-up}} = 20$ nA for the up-scan and $I_{\text{th-down}} = 120$ nA for the down-scan. For each scan rate, 500 events are considered to form the distribution function $P(E_H)$, and the total probability of $P(E_H)$ is normalized to unity. The scanning rates for S2 are usually set in the range between 1 and 200 Hz, corresponding to scan rates between 0.4 and 80 V/s. In principle, higher scanning rates extend the measurements to shorter lifetimes. However, because of limitation imposed by the bandwidth of the measurement circuit, sufficiently good statistics could be obtained only for the scan rates up to 80 V/s.

Figure 4(a) shows the distribution function $P(E_H)$ for the critical field with different scan rates. For different scan rates, the histogram peaks of $\nu \sim 2$ in Fig. 4(a) shift with faster scans. During the up-scan, the peaks of $P(E_H)$ shift towards higher E_H values, while for the down-scan, they shift towards lower values. The width of $P(E_H)$ becomes greater with faster scan rates. In contrast, $P(E_H)$ at $\nu = 4$ shown in Fig. 4(a) exhibits sharp peaks, which have width values and positions that are indistinguishable between different scan rates within the experimental error. This result suggests that the bistability region is too narrow to be experimentally resolved. The stochastic behaviors of $P(E_H)$ observed at different filling factors are coincident with the characteristics of the I_{SD}-V_{SD} curves.

The values of τ_L and τ_H can be directly derived from Eqs. (1a) and (1b) because $P(E_H)$ and dE_H/dt are known. Figure 4(b) shows the escape rates at $\nu \sim 2$ obtained from $P(E_H)$ curves shown in Fig. 4(a). The observed lifetimes τ_L and τ_H cover the range from $\sim$1 to $\sim$$10^{-5}$ s. In the bistable regime, $1/\tau_L$ rapidly increases as $E_H \gtrsim 5.5$ kV/m; meanwhile, $1/\tau_H$ drops drastically as $E_H \lesssim 6.0$ kV/m. A crossover of $1/\tau_L$ and $1/\tau_H$ occurs at $\tau_L \sim \tau_H \sim 10$ μs.

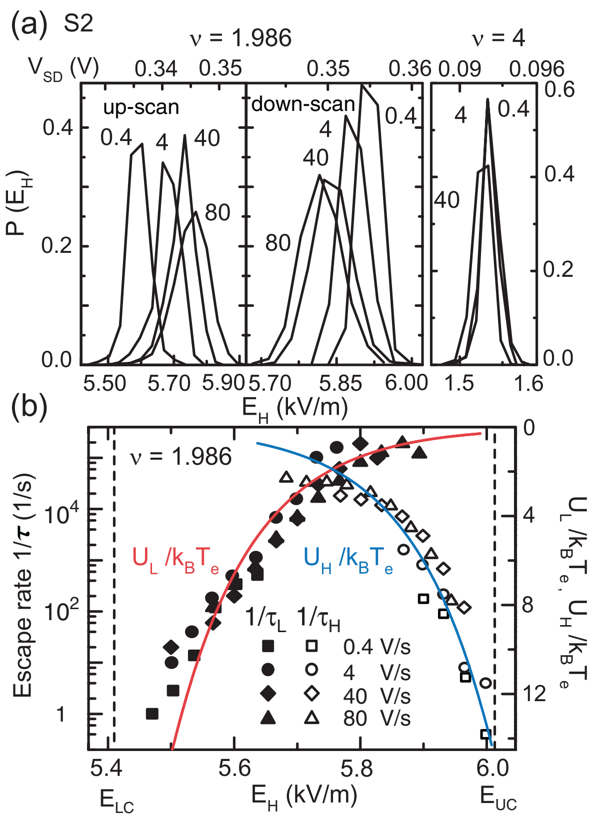

FIG. 4. (Color online) Probability density $P(I)$ vs E_H or V_{SD}, derived from 500 driving up- or down-scan waveforms. (a) $P(E_H)$ for S2 at $\nu \sim 2$. Here $E_H = V_{SD}/W$ with $W = 60$ μm for S2. (b) Escape rates $1/\tau_L$ and $1/\tau_H$ for S2 at $\nu \sim 2$ as a function of E_H, derived from the histograms shown in (a). The red and blue lines are obtained from the numerical fitting.

The extrapolations of $1/\tau_L$ and $1/\tau_H$ curves on E_H provide an estimation of the border of the bistable region: $E_{LC} \sim 5.4$ kV/m and $E_{UC} \sim 6.1$ kV/m. In the presence of bistability, the experimentally extracted values of E_{LC} or E_{UC} could be significantly different from the theoretically expected values.[28] This difference may occur because the escape rate $1/\tau_L$ (or $1/\tau_H$) could be too high to be observed for the transition to T_{HS} state (or T_{LS} state).

To provide a quantitative evaluation of the transition rate, we argue that the transition process can be viewed as a fluctuation-induced activation over an energy barrier in effective potentials U_L and U_H, manifesting the T_{LS} and T_{HS} states, respectively, as depicted in the insets of Fig. 1. The insets depict the evolution of the potential energy profile with E_H. As E_H ramps, the barrier heights of U_H and U_L change accordingly, as does the jump rate between the two valleys and the relaxation time required to reach equilibrium. Strictly, U_L and U_H should be considered in the context of nonequilibrium thermodynamics. For simplicity we assume that the probability of finding the stable state satisfies the Boltzmann distribution. The escape rates from the local stable states triggered by thermal activation can be defined as $1/\tau_L = (1/\tau_o)\exp(-U_L/k_BT_e)$ and $1/\tau_H = (1/\tau_o)\exp(-U_H/k_BT_e)$. Furthermore, we adopt an phenomenological approach and assume that U_L decreases exponentially with increasing E_H within a bistable region, $U_L/k_BT_e = t_{L0}\exp(-E_H/E_0)$; meanwhile, U_H increases exponentially with increasing E_H, $U_H/k_BT_e = t_{H0}\exp(E_H/E_0)$.[28] The theoretical fitting curves for $1/\tau_L$ and $1/\tau_H$ are shown in Fig. 4(b), in which the fitting parameters are $1/\tau_0 = 4\times10^5$ s^{-1}, $t_{L0} = 2.0\times10^{20}$, $t_{H0} = 1.8\times10^{-20}$, and $E_0 = 124.8$ V/m.

III. DISCUSSION

The experimental results shown in Fig. 4 provide compelling direct evidence that the transient of the breakdown process shows bistable behavior. Our experiments unambiguously reveal the transition dynamics of the bistable states during QHS breakdown at $\nu \sim 2$. Such bistable behavior is unobservable at $\nu \sim 4$. To further emphasize the generality of our findings, in the following we theoretically simulate the magnetic field dependence of the bistability and its dynamic properties accompany with the bistability, and we compare these calculations with the experimental results.

Based on the bootstrap electron heating model (BSEH), the bistability of the T_e-E_H relation can be naturally deduced by examining the balance condition of the energy flow between the gain rate from the Joule heat G and the loss rate caused by heat flux into the coolant L, that is, $G = L$.[17,25,31] Here $G = \sigma_{xx}E_H^2$ and $L = [Z(T_e) - Z(T_L)]/\tau_\epsilon$, where T_L is the lattice temperature, τ_ϵ represents the energy relaxation time of the heated electrons, and Z is the internal energy of the electron system. Neglecting spin splitting, Z can be expressed as $Z(T_e) = 2\int_{\epsilon_F}^{\infty}(\epsilon - \epsilon_F)D(\epsilon)f(\epsilon)d\epsilon$, where $D(\epsilon)$ is the density of states (DOS) of Landau level (LL), $f(\epsilon)$ is the Fermi distribution function, and ϵ_F is the Fermi energy.

The conductivity σ_{xx} can be derived from the determined T_e as a function of E_H:[31]

$$\sigma_{xx}(T_e) = \sigma_0\exp\left(\frac{-\Delta}{k_BT_e}\right) + \frac{\alpha}{T_e}\exp\left(-\sqrt{\frac{T_0}{T_{\rm eff}}}\right), \quad (2)$$

The first term in the sum of Eq. (2) describes the thermal activation with an activation energy of $\Delta = \hbar\omega_c/2$, and the second term is a variable-range hopping (VRH) conductivity, in which an effective temperature $T_{\rm eff} = \sqrt{T_e^2 + \zeta E_H}$ is adopted to account for LL broadening induced by heating from the electric field or E_H, which is scaled by a parameter ζ.[32] Generally, VRH conductivity dominates at lower temperatures. Based on previous studies[7,31] we estimate the relevant parameters for the calculation of σ_{xx} as follows: an LL broadening of $\Gamma = 0.035\hbar\omega_c$, a conductivity prefactor of $\alpha = 9.3\times10^{-7}$ S K, $T_0 = 13$ K, $\tau_\epsilon = 1\times10^{-8}$ s, and $\sigma_0 = 1.4\times10^{-3}$ S. ζ is an adjustable parameter in the calculation that is set at 0.01 m C K^2/J. Here we assume that $D(\epsilon)$ includes a Gaussian DOS and a constant background state with a ratio set equal to 0.15, as defined in Ref. 31. Note that all adjustable parameters of Eq. (2) in our simulation are deliberately adapted to the values closed to those used in Refs. 7 and 31 for better comparison to the previous works.

Figure 5(a) shows the calculated T_e-E_H diagrams for various values of B at $T_L = 1$ K and Fig. 5(b) shows the equivalent diagrams for various T_L values at $B = 5.76$ T. The balance between G and L yields an S-shaped dependence of E_H on T_e, shown in Fig. 1. The occurrence of bistable states and the width of the bistable region with respect to E_H

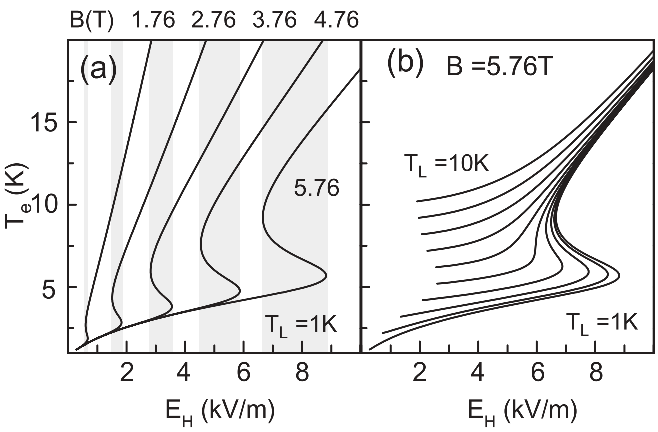

FIG. 5. Calculated electron temperature T_e vs E_H curves obtained using the power-balance equation. (a) Traces for different magnetic fields at a lattice temperature of $T_L = 1$ K. The shaded area in a given B represents the bistable regime of T_e. (b) Traces for different T_L at $B = 5.76$ T, where T_L is stepped by 1 K between traces.

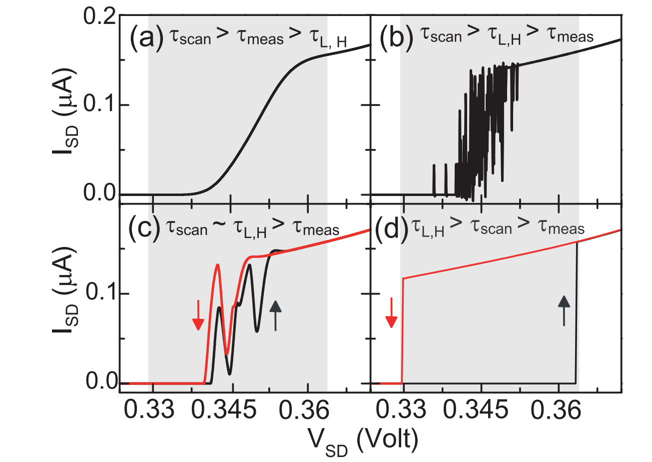

FIG. 6. (Color online) The simulated I_{SD}-V_{SD} curves for (a) $\tau_{\mathrm{scan}} > \tau_{\mathrm{meas}} > \tau_L, \tau_H$, (b) $\tau_{\mathrm{scan}} > \tau_L, \tau_H > \tau_{\mathrm{meas}}$, (c) $\tau_{\mathrm{scan}} \sim \tau_L, \tau_H > \tau_{\mathrm{meas}}$, and (d) $\tau_L, \tau_H > \tau_{\mathrm{scan}} > \tau_{\mathrm{meas}}$. The shaded areas bounded by $V_{\mathrm{SD}} \sim E_{\mathrm{LC}} W$ and $\sim E_{\mathrm{UC}} W$ mark the bistable regimes.

evolve with variation of B and T_L. The S characteristic of the bistable regime is reduced as B decreases or T_L increases. This relationship provides an experimental explanation for the fact that bistability is frequently observed at higher B (lower ν, e.g., $\nu = 2$) but is less likely at lower B (higher ν, e.g., $\nu = 4$, 6). The bistable region disappears for $T_L \geqslant 7$ K in Fig. 5(b), at which point thermal activation conductivity dominates σ_{xx}.

On the other hand, the ostensible absence of instability of I_{SD} in S3 as shown in Fig. 3(d) can be understood by considering the spatial evolution of the heating processes.[26] With increasing E_H the dissipative region will extend across the full width of the conductor, and spatially homogeneous dissipation state would be easier achieved for narrower W. As a result, a narrower Hall bar usually gives rise to a smaller bistable regime.

To understand the transient behavior of I_{SD} across the bistable region observed in the experiments, the time scales associated with the measurement must be considered together with the intrinsic lifetimes of the system (τ_L and τ_H). The time scales of interest include τ_{scan} and τ_{meas}, which refer to the ramping rate of E_H and the bandwidth of the measurement circuit, respectively. In general, the instrument setting must ensure that $\tau_{\mathrm{scan}} \gg \tau_{\mathrm{meas}}$ to collect meaningful data. For the I_{SD}-V_{SD} curves shown in Fig. 3(b), $\tau_{\mathrm{scan}} \approx 30$ s and $\tau_{\mathrm{meas}} \approx 0.5$ s for 33.3 mV/s, $\tau_{\mathrm{scan}} \approx 1$ s and $\tau_{\mathrm{meas}} \approx 0.01$ ms for 0.4 V/s, and $\tau_{\mathrm{scan}} \approx 0.01$ s and $\tau_{\mathrm{meas}} \approx 0.01$ ms for 40 V/s. Clearly, as $\tau_{\mathrm{scan}} > \tau_{\mathrm{meas}} > \tau_{L,H}$, I_{SD} exhibits a smooth transition, which suggest that fluctuations of I_{SD} between bistable states are averaged out for longer τ_{meas}. In contrast, as $\tau_{\mathrm{scan}} > \tau_{L,H} > \tau_{\mathrm{meas}}$, an individual transit event can be resolved in the measurement; consequently, telegraph-like switching behaviors of I_{SD} are observed.

To further verify our interpretations, we simulate the I_{SD}-V_{SD} traces over a broader time scale. For a given E_H (or V_{SD}) in the bistable regime, we assume that σ_{xx} (or I_{SD}) is either zero with a lifetime of τ_L at the T_{LS} state or a dissipative resistor with a finite value, $\sigma_{xx} \sim 24.9$ nS (derived from Fig. 3(b) with $I_{\mathrm{SD}} \sim 0.17$ μA at $V_{\mathrm{SD}} \sim 0.365$ V), with a lifetime of τ_H at the T_{HS} state. Furthermore, we consider the transition is randomly triggered, and the system stay in either the T_{LS} or T_{HS} state, with the probability given by $\tau_L/(\tau_L + \tau_H)$ or $\tau_H/(\tau_L + \tau_H)$, respectively. Then the value of I_{SD} at any given V_{SD} within the bistability regime can be obtained by knowing τ_L, τ_H, and τ_{meas}. The behaviors of τ_L and τ_H as a function of V_{SD} are obtained from Fig. 4(b). As V_{SD} ramps up with a given τ_{scan}, we can calculate I_{SD}. Experimentally the upper limit of τ_{scan} and τ_{meas} are restricted by instruments and circuit, that is, $\tau_{\mathrm{scan}} < 0.005$ s, $\tau_{\mathrm{meas}} < 10^{-5}$ s. However, to explore all possible transient response, we can choose the wider values of these parameters; in particular for higher scan rate and measurement speed. The relevant simulation parameters are set within $\tau_{\mathrm{scan}} \sim 10$–$2 \times 10^{-4}$ s, $\tau_{\mathrm{meas}} \sim 0.3$–$10^{-7}$ s, and $\tau_{L,H} \sim 4 \times 10^{5}$–$2.6 \times 10^{-6}$ s. The simulated I_{SD}-V_{SD} curves for the condition $\tau_{\mathrm{scan}} > \tau_{\mathrm{meas}} > \tau_L, \tau_H$ are shown in Fig. 6(a), $\tau_{\mathrm{scan}} > \tau_L, \tau_H > \tau_{\mathrm{meas}}$ are shown in Fig. 6(b), $\tau_{\mathrm{scan}} \sim \tau_L, \tau_H > \tau_{\mathrm{meas}}$ are shown in Fig. 6(c), and $\tau_L, \tau_H > \tau_{\mathrm{scan}} > \tau_{\mathrm{meas}}$ are shown in Fig. 6(d). If τ_{meas} is much longer than τ_L and τ_H, the fluctuating nature of a bistable state can be completely averaged out. A smooth I_{SD}-V_{SD} curve is found, as shown in Fig. 6(a). Nevertheless, when τ_L or τ_H is larger than or comparable to τ_{meas}, I_{SD} is determined by how often the system stays at the T_{HS} state, that is, $\tau_H/(\tau_L + \tau_H)$, how long the system retains at the given V_{SD}, that is, τ_{scan}, and the duration of a measurement, that is, τ_{meas}. The interplay among τ_L, τ_H, τ_{meas}, and τ_{scan} will give rise to different fluctuating I_{SD}-V_{SD} behaviors, as shown in Figs. 6(a)–6(c). The calculated traces reproduce the features of I_{SD}, which are displayed in Fig. 3(b). Moreover, Fig. 6(d) exhibits a distinct hysteresis, the width of which is bounded by E_{LC} and E_{UC}. The quantities τ_H and τ_L are material parameters, the values of which vary in different samples. Our results provide a consistent interpretation to account for a wide variety of the features of the previously reported QHE breakdown.

Finally, we wish to comment on recent series of works by Refs. 7 and 22. Kalugin *et al.* reported experimental observations of the frequency dependence of the breakdown hysteresis by direct measurements of the ac response of current-voltage breakdown curves measured at $\nu = 2$ in a

Carbino QH device.[22] As the applied voltage amplitude exceeds the upper hysteresis limit $V_{\max}$, the hysteresis amplitude ($V_{\max} - V_{\min}$) grows drastically as the frequencies increase in the low-frequency range, and it saturates at higher frequencies (>20 Hz), where $V_{\min}$ represents the lower hysteresis limit.[22] Later, Buss and co-workers further demonstrated the existence of a pre-breakdown σ_{xx}, at which ac values steeply drop below their dc counterparts at frequencies below 20 Hz.[7] Accordingly, they suggested that the observed dynamical hysteresis and frequency dependence of σ_{xx} can be attributed to the suppressed delocalization of electrons under an ac driving electric field, which is caused by the frequency dependence of VRH conductivity at low temperatures. Compared to the observed ramping rate dependence of the $P(E_H)$ peak shown in Fig. 4(a), the shift of the histogram peak to larger (smaller) values of E_H with higher scan rate during up-scan (down-scan) fits the general descriptions of the frequency dependence of $V_{\max}$ and $V_{\min}$ in Ref. 22. We can reproduce observations similar to those of Ref. 7 in the S2 sample. For $V_{\mathrm{SD(rms)}} = 0.38$ V and a critical voltage of 0.46 V at 1.86 K, σ_{xx} is found to decrease sharply for frequencies up to 10 Hz. However, a closer examination of our experimental conditions and those in Ref. 7 reveal that the amplitude of V_{SD} is actually larger than the critical voltage. In view of these findings, we suggest that the observed frequency dependencies of the dynamical hysteresis and σ_{xx} are simply a result of the transient dynamics associated with the bistability of the breakdown states, as discussed above.

IV. CONCLUSIONS

We investigate the transition dynamics associated with the integer QHE breakdown in Corbino devices. The transient behaviors that occur during the breakdown process are studied by applying a source-drain bias with different scan rates. The critical E_H at $\nu \sim 2$ is found to fluctuate and depend on the scan rate; however the same phenomenon is not observed at $\nu \sim 4$. The histograms of the fluctuating E_H are recorded, and they reveal the stochastic nature of the transition. The escape rates between the low-dissipative QHS and the dissipation states are derived as a function of E_H, ranging from approximately a few seconds to a few microseconds. Theoretical simulations based on the BSEH model are employed, and they are in agreement with the experimental findings. Finally, we demonstrate that various breakdown features observed can be consistently interpreted by considering the relevant time scales in the experimental system.

ACKNOWLEDGMENTS

We acknowledge Y. P. Lin for experimental assistance and Po-Chung Chen for helpful discussions. This work is supported by the National Science Council (No. NSC 95-2112-M-007-049-MY3) in Taiwan, the Boost project of the University, and a Grant-in-Aid for Scientific Research (A,19204031) from the Japan Society for the Promotion of Science (JSPS).

[1] S. Kawaji and J. Wakabayashi, in *Physics in High Magnetic Fields*, edited by S. Chikazumi and N. Miura (Springer, Berlin, 1981), p. 284.
[2] K. V. Klitzing, G. Dorda, and M. Pepper, Phys. Rev. Lett. **45**, 494 (1980).
[3] G. Ebert, K. von Klitzing, K. Ploog, and G. Weimann, J. Phys. C **16**, 5441 (1983).
[4] M. E. Cage, R. F. Dziuba, B. F. Field, E. R. Williams, S. M. Girvin, A. C. Gossard, D. C. Tsui, and R. J. Wagner, Phys. Rev. Lett. **51**, 1374 (1983).
[5] R. Woltjer, R. Eppenga, J. Mooren, C. Timmering, and J. Andre, Europhys. Lett **2**, 149 (1986).
[6] P. G. N. deVegvar, A. M. Chang, G. Timp, P. M. Mankiewich, J. E. Cunningham, R. Behringer, and R. E. Howard, Phys. Rev. B **36**, 9366 (1987).
[7] A. Buss, F. Hohls, F. Schulze-Wischeler, C. Stellmach, G. Hein, R. J. Haug, and G. Nachtwei, Phys. Rev. B **71**, 195319 (2005).
[8] F. J. Ahlers, G. Hein, H. Scherer, L. Bliek, H. Nickel, R. Lösch, and W. Schlapp, Semicond. Sci. Technol. **8**, 2062 (1993).
[9] G. Boella, L. Cordiali, G. Marullo-Reedtz, D. Allasia, G. Rinaudo, M. Truccato, and C. Villavecchia, Phys. Rev. B **50**, 7608 (1994).
[10] M. E. Cage, J. Res. Natl. Inst. Stand. Technol. **98**, 361 (1993).
[11] D. C. Tsui, G. J. Dolan, and A. C. Gossard, Bull. Am. Phys. Soc. **28**, 365 (1983).
[12] O. Heinonen, P. L. Taylor, and S. M. Girvin, Phys. Rev. B **30**, 3016 (1984).
[13] L. Eaves and F. W. Sheard, Semicond. Sci. Technol. **1**, 346 (1986).
[14] O. Makarovsky, A. Neumann, L. A. Dickinson, L. Eaves, P. C. Main, M. Henini, S. Thoms, and C. D. W. Wilkinson, Physica E **12**, 178 (2002).
[15] L. Eaves, Physica B **298**, 1 (2001).
[16] P. Středa and K. von Klitzing, J. Phys. C **17**, L483 (1984).
[17] S. Komiyama, T. Takamasu, S. Hiyamizu, and S. Sasa, Solid State Commun. **54**, 479 (1985).
[18] T. Takamasu, S. Komiyama, S. Hiyamizu, and S. Sasa, Surf. Sci. **170**, 202 (1986).
[19] G. Nachtwei, G. Lutjering, D. Weiss, Z. H. Liu, K. V. Klitzing, and C. T. Foxon, Phys. Rev. B **55**, 6731 (1997).
[20] A. Vl. Gurevich and R. G. Mints, Pis'ma Zh. Eksp. Teor. Fiz. **39**, 318 (1984) [JETP Lett. **39**, 381 (1984)].
[21] V. Tsemekhman, K. Tsemekhman, C. Wexler, J. H. Han, and D. J. Thouless, Phys. Rev. B **55**, 10201R (1997).
[22] N. G. Kalugin, B. E. Sağol, A. Buß, A. Hirsch, C. Stellmach, G. Hein, and G. Nachtwei, Phys. Rev. B **68**, 125313 (2003).
[23] Y. Kawaguchi, F. Hayashi, S. Komiyama, T. Osada, Y. Shiraki, and R. Itoh, Jpn. J. Appl. Phys. **34**, 4309 (1995).
[24] Y. Kawaguchi, S. Komiyama, T. Osada, and Y. Shiraki, Physica B **227**, 183 (1996).
[25] S. Komiyama, Y. Kawaguchi, T. Osada, and Y. Shiraki, Phys. Rev. Lett. **77**, 558 (1996).
[26] G. Nachtwei, Physica E **4**, 79 (1999).
[27] R. Landauer, Phys. Today **31**(11), 23 (1978).
[28] T. Nakajima and S. Komiyama, Physica E **42**, 1026 (2010).
[29] A. V. Gurevich and R. G. Mints, Rev. Mod. Phys. **59**, 941 (1987).
[30] T. A. Fulton and L. Dunkleberger, Phys. Rev. B **9**, 4760 (1974).
[31] S. Komiyama and Y. Kawaguchi, Phys. Rev. B **61**, 2014 (2000).
[32] D. G. Polyakov and B. I. Shklovskii, Phys. Rev. Lett. **70**, 3796 (1993).